IEEE Access
Multidisciplinary ⋮ Rapid Review ⋮ Open Access Journal

Received 16 July 2025, accepted 12 August 2025, date of publication 21 August 2025, date of current version 27 August 2025.

Digital Object Identifier 10.1109/ACCESS.2025.3601378

RESEARCH ARTICLE

Frequency Regulation Analysis of the Coca Codo Sinclair Hydropower Plant (Ecuador) in Isolated Operation With High Wind Power Penetration

GUILLERMO MARTÍNEZ-LUCAS[1], ANA FERNÁNDEZ-GUILLAMÓN[2,3], VICTOR A. GALLO MIER[1], AND JOSÉ IGNACIO SARASUA[1]

[1]Department of Hydraulic, Energy and Environmental Engineering, Universidad Politécnica de Madrid, 28040 Madrid, Spain
[2]Faculty of Engineering, Distance University of Madrid (UDIMA), Collado Villalba, 28400 Madrid, Spain
[3]Department of Applied Mechanics and Projects Engineering, Renewable Energy Research Institute, Universidad de Castilla–La Mancha, 02071 Albacete, Spain

Corresponding author: Ana Fernández-Guillamón (ana.fguillamon@uclm.es)

This work was supported by Madrid Government (Comunidad de Madrid-Spain) through the Multiannual Agreement 2023–2026 with the Universidad Politécnica de Madrid in the Line A, Emerging Ph.D. researchers, under Grant DOCTORES-EMERGENTES-24-Y8X7NY-18-RPLBQC.

ABSTRACT The increasing integration of wind energy into isolated power systems presents significant challenges for frequency regulation, particularly in regions where renewable penetration is expected to rise. This paper analyzes the frequency control capabilities of the Coca Codo Sinclair Hydropower Plant under such conditions, proposing a systematic methodology for tuning the gains of its speed governor. A dynamic model of the plant is developed in Matlab Simulink, explicitly incorporating long penstocks and hydraulic coupling between generating units, a configuration rarely addressed in conventional tuning approaches. The tuning strategy is based on minimizing a performance penalty index that reflects the plant's response to power disturbances. Two gain-setting approaches are evaluated: one that adapts to the operational configuration of the generation units, and another that uses fixed gains regardless of operating mode. Simulation results, aligned with national renewable expansion plans, show that both strategies improve frequency stability compared to conventional tuning. The mode-dependent tuning yields better performance in reducing frequency deviations, while the fixed-gain approach simplifies implementation but may increase mechanical stress on turbine components. The results demonstrate that a suitable methodology for tuning speed controller gains in isolated systems with complex hydraulic dynamics enhances system performance, even under high wind power penetration levels. Moreover, these results highlight the importance of realistic modeling and adaptive tuning in the reliable integration of renewable energy in remote and decarbonization-priority areas.

INDEX TERMS Frequency control, governor tuning, hydropower plant, isolated power system, pelton turbine, renewable energy integration.

I. INTRODUCTION

The growing integration of renewable energy sources into power systems (mainly wind and solar) due to the global shift towards decarbonization [1] has highlighted the challenges of maintaining grid stability [2], particularly in isolated grids [3]. However, the integration of these intermittent renewables has intensified the need for reliable and flexible generation resources to compensate for their variability [4]. Hydropower plants play a crucial role in this context [5]; being also based on a renewable resource and offering fast frequency response, they can provide a solution to continue with climate change mitigation while ensuring system stability [6], [7]. However, frequently adjusting the hydropower plant's setpoint can lead to water hammer (especially when the penstocks are very long), resulting in pressure and stress transients within the pressurized conduits, particularly in the penstock [8]. These pressure oscillations

The associate editor coordinating the review of this manuscript and approving it for publication was Ahmed A. Zaki Diab.

make frequency control very difficult, due to the effect that the inertia of the water reduces the speed of response of the mechano-hydraulic regulators.

To overcome this, the proper tuning of hydroelectric plant controllers is critical to achieving a stable and efficient frequency response: an inadequately adjusted governor can lead to excessive oscillations, slow recovery, or even instability, particularly under sudden load changes or renewable generation fluctuations. As a consequence, lots of papers have focused on proposing governor tuning methodologies for hydropower plants. Despite the recent technological changes, PID controllers are still used in most hydroelectric power plants. Consequently, research is focused on studying and proposing new criteria for the adjustment of controller gains or methodologies for their determination. For instance, some recent proposals include a two-step method to tune PID and droop compensator to enhance frequency control [9]; a self-tuning fuzzy PD controller for load frequency control in a microgrid with high penetration of mini-hydropower [10]; advanced optimization techniques (including multiple objective particle swarm optimization, genetic algorithms, bees, and reinforcement learning) to optimize controller gains based on frequency sensitivity margins and error metrics to improve frequency control [11]; a combination of fuzzy logic and PID control optimized via particle swarm optimization [12]; and a robust sliding mode control method with a PID-based sliding surface for frequency regulation in multi-area power systems [13].

Even though the presence of long penstocks introduces complex hydraulic dynamics that can affect the performance of frequency control [14], and many studies have modeled the dynamic behavior of hydropower plants considering such effects [15], [16], [17], [18], [19], few have addressed tuning the PID governor gains under these conditions. Reference [20] analyzed how long penstock dynamics (specifically water inertia and head loss) affect frequency regulation and stability in turbine governing systems. In [21], an improved PI governor tuning was presented by using a corrected second-order model. Sarasua et al. [22] proposed and compared two PI governor tuning methods (based on root locus and Pareto optimization) using performance metrics and simulations, showing improved load–frequency control. Similarly, [23] analyzed frequency regulation in pumped–storage plants with long penstocks and shared conduits, showing that hydraulic coupling and governor settings significantly affect system stability, providing control strategy recommendations to improve frequency response. More recently, [24] emphasized the need for advanced control techniques to optimize hydropower plant performance. Cassano et al. [25] proposed two control algorithms to mitigate pressure fluctuations and reduce penstock fatigue: a linear signal filter and a fatigue-aware method that filters out damaging control patterns based on a simplified plant model. Other authors [26] evaluated the system eigenvalues by developing a state-space model, identifying stability characteristics across various regulating regions and validating them through time-domain simulations.

Electrically isolated systems are not only found on islands. A region can become electrically isolated following a transmission network failure, either due to the disconnection of a specific area from the rest of the grid or after a system-wide blackout. In the latter case, certain power plants equipped with black-start capability gradually restore the electric system, initially supplying power to a limited number of critical loads [27]. Additionally, a region may operate as an isolated system due to the high cost or technical difficulty of constructing transmission lines. In such cases, small thermal power stations—typically diesel generator sets—are deployed to meet local demand and ensure supply to consumers in the area [28]. However, efforts are also being made to replace these diesel generators with renewable energy sources in such areas [29]. This is the case of Ecuador, a country with an extensive transmission network, but which also has electrically isolated regions, such as the Amazon provinces of Orellana and Sucumbíos, where there is a high presence of small diesel power plants [30], as shown in Fig. 1. If these electrically isolated regions were to be decarbonized, as per the country's goal [31], focusing on renewable energy sources such as hydroelectric (Coca Codo Sinclair hydropower plant) and wind power, they should be connected to the existing 230 kV transmission line.

FIGURE 1. Map of the location of thermal power plants in ecuador [30].

If this line fails, all connected elements would be disconnected from the power grid, forming an isolated electrical system. In this scenario, the Coca Codo Sinclair Hydroelectric Power Plant would be solely responsible for frequency regulation, compensating for fluctuations caused by both demand variations and wind power generation.

This would represent the most demanding scenario for the power plant in terms of frequency regulation.

In light of this context, this paper proposes a methodology for adjusting the controller of the Coca Codo Sinclair Hydroelectric Power Plant for isolated operation. The proposed approach considers all possible combinations of generating unit connections and their dynamic interactions dictated by the hydraulic circuit configuration. Despite the extensive literature reviewed, no study has been found that addresses the tuning of a hydroelectric plant operating in island mode with long pressurized conduits, while also considering the interaction among the multiple generating units. Although many references emphasize the critical influence of conduit length, only [23] explicitly considers the coupling between generating units, and even then, the isolated nature of the system is not taken into account. This highlights the originality of the present work. When penstocks are long, the configuration of generating unit connections becomes a key factor in controller tuning, as will be demonstrated throughout this paper. To address these challenges, this work proposes a methodology aimed at enhancing frequency stability in isolated hydroelectric systems with long conduits. By explicitly incorporating the hydraulic interactions between generating units and improving the dynamic response of the plant, the proposed method contributes to the broader effort of integrating renewable energy while maintaining grid reliability.

Therefore, the main contributions of this paper lie in the development and application of a tuning methodology for the Coca Codo Sinclair Hydroelectric Power Plant in Ecuador. The methodology is implemented using a detailed dynamic model built in the Matlab/Simulink environment, and considers the plant operating as an isolated power system: a scenario that represents the most demanding case for frequency regulation, especially under potential transmission line failures. Furthermore, the study incorporates national energy planning efforts, including the expansion of wind generation and the decarbonization of isolated Amazonian regions.

The rest of the paper is organized as follows: Section II describes the power system of Ecuador, as well as the Coca Codo Sinclair hydropower plant. In Section III, the methodology used in this work is detailed, including the process for obtaining the gains from the power plant controller; Section IV details and discusses the results obtained; finally, the conclusions are given in Section V.

II. POWER SYSTEM AND POWER PLANT DESCRIPTION

According to [30], the Ecuadorian power system has a total installed capacity of approximately 8,900 MW, of which 5,459 MW correspond to renewable energy sources. Among the various renewable generation technologies, 5,192 MW come from hydroelectric power plants, including both reservoir and run-of-river types, 144 MW from biomass, and the remainder from wind and photovoltaic farms. Furthermore, according to [31], the system-wide demand is projected to grow between 2018 and 2027 by 5.18% to 11.08%, depending on the scenario considered. As a result, Ecuador's main objective for the development of its power system is to ensure a reliable electricity supply through the optimal expansion of power generation, while promoting the use of renewable energy resources.

In addition to its strong commitment to hydropower, Ecuador is also conducting studies to expand wind energy generation. According to [32], the country has a short-term wind potential estimated at 1,670 MW, which could generate more than 2,800 GWh annually. This wind potential is primarily located in provinces traversed by the mountain ranges running from north to south across the country. One such province with high wind potential is Pichincha, with an estimated annual output of over 210 GWh.

In the neighboring province of Napo, near the area identified as optimal for wind turbine deployment in Pichincha, the Coca Codo Sinclair hydropower plant is located, which is the largest hydroelectric plant in Ecuador. This province borders the Amazonian provinces of Orellana and Sucumbíos to the east, where there is a high concentration of small diesel power plants, see Fig. 1. Specifically, the province of Orellana generates 78.49 MW distributed across more than 25 plants, while Sucumbíos produces 73.28 MW in over 11 facilities. Due to their location in the Amazon region, most of these small plants operate as electrical islands, disconnected from the Ecuadorian national grid and therefore supplying electricity directly to their local loads (see Fig. 1).

If these electrically isolated regions were to pursue decarbonization through the adoption of renewable energy sources such as hydro and wind power, they would need to be connected—due to geographical proximity—to the existing 230 kV transmission line that runs from Pichincha province to Shushufindi, where the line terminates. Likewise, any wind farms built on the eastern slope of the mountain range that crosses the province of Pichincha (where most of the province's wind potential is concentrated) would also be connected to this same transmission line, given the topographical constraints (see Fig. 2). Note that the Coca Codo Sinclair hydroelectric plant is connected to this same line.

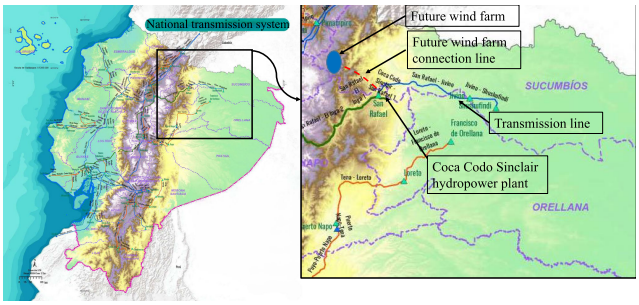

FIGURE 2. Map of the transmission lines of the Ecuadorian electrical system [30], the area with wind potential in Pichincha, and the proposed connection to the existing transmission network.

For these reasons, this transmission line is considered to be of high importance and critical infrastructure, as it would potentially carry large power flows to a densely

populated area. Therefore, among other studies that should be undertaken, it is essential to ensure the operation of this line and the uninterrupted supply of electricity to all loads in the event of a disconnection from the national transmission system. In such a scenario, both the Pichincha wind farm and the Coca Codo Sinclair hydropower plant would be isolated from the grid, and the latter would be responsible for providing the necessary regulation to allow continued operation as an isolated system. This situation would be the most demanding in terms of regulation for the hydropower plant.

Coca Codo Sinclair hydropower plant has a nominal production capacity of 1,500 MW distributed among 8 Pelton turbines, a head of 620 meters, and an operational flow of 278.50 m^3/s [30]. The plant supplies over 36% of the annual energy demand of the country and has reached 57% [33]. Since its commissioning in 2016, Coca Codo Sinclair has significantly enhanced Ecuador's electricity generation capacity, reducing its dependence on imported energy and fossil fuel consumption. This has led to economic savings by reducing fuel subsidies and imports of diesel and naphtha for thermal power plants [34].

The hydraulic circuit of the hydroelectric power plant begins with a dam on the Coca River, which captures the water. The headrace tunnel, entirely constructed underground and lined with concrete, has an internal diameter of 8.20 meters. The water travels under free-surface conditions along its 24.83-kilometer length towards a forebay. This forebay has a capacity of 0.80 hm^3. From the forebay, the penstocks transport the water to the turbines. This hydraulic configuration can be seen in Fig. 3.

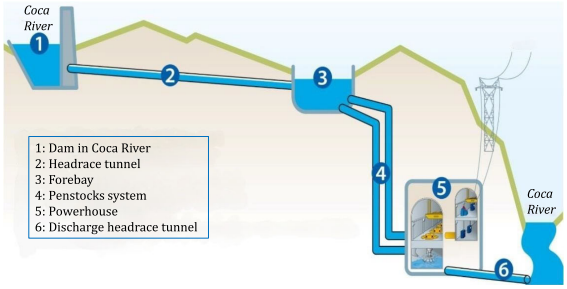

FIGURE 3. Sketch of the Coca Codo Sinclair hydroelectric power plant.

The penstock system of the Coca Codo Sinclair Hydroelectric Power Plant is divided into two hydraulic circuits, each featuring a main penstock with lengths of 1,469 m and 1,462 m, respectively. These penstocks are lined with concrete to ensure durability and structural resistance, a standard approach in large-scale hydroelectric plants to prevent the wear and degradation of materials [35]. Both pipes have an internal diameter of 5.80 m, allowing the transport of large volumes of water. However, in the last 400 m of their path, the internal diameter is reduced to 5.20 m and is lined with steel, allowing a smooth transition of the flow and minimizing energy losses, a design feature aimed at improving the efficiency of the system [36]. Upon reaching the powerhouse, these two main penstocks split into four branches each, resulting in a total of eight branches that distribute water to the Pelton turbines. Each turbine operates at a speed of 300 revolutions per minute (rpm) and is equipped with six injectors, generating 187.50 MW per unit. In total, these generators produce a nominal power output of 1,500 MW, characteristic of the high-efficiency configuration found in the Coca Codo Sinclair plant, which uses Pelton turbines for its large-scale electricity production [37].

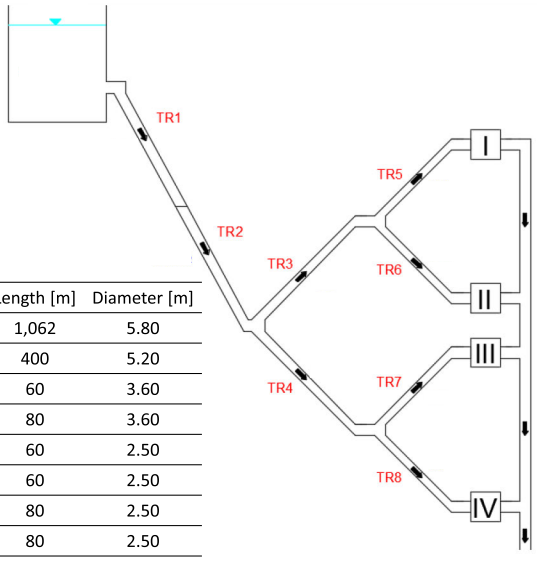

Section	Length [m]	Diameter [m]
TR1	1,062	5.80
TR2	400	5.20
TR3	60	3.60
TR4	80	3.60
TR5	60	2.50
TR6	60	2.50
TR7	80	2.50
TR8	80	2.50

FIGURE 4. Hydraulic scheme of the Coca Codo Sinclair power plant and conduits data.

III. METHODOLOGY

To achieve the goals previously described, the Coca Codo Sinclair hydropower plant connected to an isolated system have been modeled in MATLAB with Simulink, as described in Section III-A. The construction of a realistic model that accurately represents all the phenomena involved in system operation is crucial to obtain meaningful conclusions [38]. The power plant would be the only generation plant supplying the net demand, i.e. the residual demand remaining after subtracting the intermittent wind generation. This hypothesis, which has been assumed in other works [39] implies that wind and solar generation do not contribute to frequency regulation; this service being exclusively provided by the hydroelectric power plant. Furthermore, wind turbines in wind farms are typically connected to the grid through power electronic converters, which decouple their mechanical inertia from the grid and, as a result, do not contribute to system inertia.

A. DYNAMIC MODEL

In addition to the electrical system itself, the dynamic model developed must include those hydraulic elements that affect the dynamic response of the power plant in the time range of a few seconds. In this case, the dynamic phenomena that occur in the tunnel and in the two reservoirs have been omitted.

For this reason, the model includes the forebay as a constant water level, all the penstocks, as well as the bifurcations until the water is conveyed to the eight turbines, which have also been modelled. The schematic of the modelled elements can be seen in Fig. 4, as well as the lengths and diameters of each section of the conduits. The hydraulic configuration of the power plant includes large penstocks, which limits the applicability of rigid-water column models and requires consideration of elastic effects [40].

As mentioned earlier, the hydropower plant operates within an isolated system that includes intermittent energy sources and a constant power demand. The frequency dynamics, as described by (1), result from the imbalance between the combined power output of the hydroelectric plant ($\sum p_{h,i}$) and wind farms (p_w), and the power demand (p_{dem}).

$$f\frac{df}{dt} = \frac{1}{\sum 2H_{h,i}}\left(\sum p_{h,i} + p_w - p_{dem}\right) \tag{1}$$

The system's inertial response is attributed solely to the hydropower plant, as the wind farms are connected via a frequency converter and does not contribute to system inertia, so that the inertia constant $2H_{h,i}$ refers only to each hydraulic turbines on line at any given time.

Transient flow in conduits is described by the conservation of mass and momentum as described in [41]. Different approaches can be found in the specialized literature to solve these equations such as the method of characteristics [42] or the transfer function proposed in [15]. However, The lumped parameter approach has been used in this work as in previous studies as [18].

This method results in a system of ordinary differential equations that can be depicted as a sequence of consecutive Γ-shaped elements. In this representation, the conduit's properties—such as inertia, elasticity, and friction—are distributed in proportion to the segment length L_e. The 'arrangement' and 'orientation' of these Γ-shaped elements may change depending on the boundary conditions at the upstream and downstream ends of the pipe. Therefore, the governing equations for the penstock dynamics are (2) and (3), where T_w represent the water starting time, defined in (4).

$$\frac{dq_{p,m}}{dt} = \frac{n_t}{T_w}(h_m - h_{m+1} - \frac{r}{2n_t}q_{p,m}|q_{p,m}|) \tag{2}$$

$$\frac{dh_m}{dt} = n_t\frac{T_w}{T_e^2}(q_{p,m} - q_{p,m+1}) \tag{3}$$

$$T_w = \frac{L}{gS}\frac{Q_b}{H_b} \tag{4}$$

The order of the system is defined by the total number of segments ($\sum n_t$) along the entire pipeline. In this case, segments TR1 and TR2 — which differ in both length and construction material, as shown in Fig. 4 — have been discretized into four segments each, while in the rest of the sections (i.e. TR3 to TR8) a single segment has been considered.

The turbine is modeled according to the recommendations of [15]. Equation (5) defines the relationship between the flow rate (q_i), net head (h_i), and nozzle opening (z_i), while (6) provides the generated power based on the flow rate, net head, frequency variation (Δf), and nozzle opening. Additionally, A_t and D_t, correspond to turbine parameters while q_{nl} corresponds to the no load flow.

$$q_i = z_i\sqrt{h_i} \tag{5}$$

$$p_{h,i} = A_t h_i(q_i - q_{nl}) - D_t z_i \Delta f \tag{6}$$

The hydroelectric governor model, widely used in the scientific literature and in hydropower plants, is expressed in (7). Its key role is to regulate the unit speed by adjusting the turbine nozzles and managing the water flow through the penstock based on the feedback frequency error signal. This signal is processed using a standard proportional–integral (PI) controller. To account for operational constraints, the model includes a rate limiter and a saturator element, which restrict the nozzle positions and their rate of change.

$$\Delta z_i = \left(K_p + K_i\int dt\right)\Delta f \tag{7}$$

B. POWER PLANT OPERATING MODES

To ensure post-fault stability in isolated operation, several configurations were analyzed at 45% capacity per unit, enabling the plant to restore supply progressively after a system outage. In this way, the plant could supply a minimum output of 84.375 MW with a single on - line unit. Due to the configuration of the hydraulic system, only the operating combinations of units 1 to 4 need to be analysed, as units 5 to 8 are hydraulically independent and would not interact with each other. A summary of the plant operating configurations can be seen in Table 1. The analysis of configurations 3, 4 and 5, which might appear to be equivalent, is performed to assess the impact of the penstock bifurcations on the controller setting. Although the settings obtained are expected to be very similar, it is essential to verify this hypothesis by means of a detailed study. Similarly, the same approach is followed for configurations 6 and 7.

TABLE 1. Operating point of each hydroelectric power unit for each mode of operation.

Operating mode	Group I	Group II	Group III	Group IV
1	45%	45%	45%	45%
2	45%	45%	45%	—
3	45%	45%	—	—
4	—	—	45%	45%
5	45%	—	—	45%
6	—	—	—	45%
7	—	45%	—	—

C. GOVERNOR GAINS SETTING FOR EACH OPERATING MODE: MODE-DEPENDENT TUNING

The correct tuning of the controller gains is essential in hydraulic systems with long pipelines, since classic recommendation for isolated system proposed by Paynter [43] does not take into account the elasticity of both the water and

the pipes [21]. In this context, it is highlighted that, in long conduits, the interaction between the elasticity of the fluid and the structure of the conduits significantly influences the dynamics of the system, generating oscillations and pressure variations that do not manifest themselves in short conduits. In fact, it has been shown that these pressure oscillations occurring in the penstock are transferred to the power system through fluctuations in the frequency [44]. Since Paynter's adjustment omits these factors, it is considered to have room for improvement. Therefore, an alternative calibration of the regulator is essential to compensate for these elastic effects, thus ensuring an optimal and stable performance of the hydraulic system.

A methodology based on exhaustive searches is proposed for the adjustment of the hydropower plant controller gains for each of the configurations presented above. To obtain the governor gains for the configurations described previously, several exhaustive searches had been carried out by varying the hydropower controller gains when a 5% step increase in the power supplied had been simulated, according to the recommendation in [45] for the speed governor of hydraulic turbines.

The study ranges of the gains have been in all cases equal, having varied for K_p between 1.30 and 2.30 while for K_i having varied between 0.14 and 0.44. It has been verified that gains outside of these bounds can destabilize the system.

NADIR and frequency settling time t_s are technical indicators used to differentiate the guaranteed frequency operating range of the system from the non-guaranteed one when there is a sudden change in power demand. These indicators can be applied in any power network to assess frequency response following a generator outage [46]. In this context, the settling time t_s refers to the time it takes for the frequency to return within the normal range set by Ecuador's Transmission System Operator (TSO) [47], which corresponds to a ± 150 mHz band. Identifying a set of controller gains that simultaneously optimizes both indicators is essential for the proper development of the hydropower plant. To address this and enhance response quality, a penalty parameter has been introduced, which increases with higher values of t_s and NADIR, as formulated in (8). Therefore, the control objective becomes the minimization of this parameter.

$$\phi = \frac{t_s}{nadir} \tag{8}$$

Therefore, NADIR, frequency settling time t_s, and the ϕ coefficient are employed to assess the quality of the system's response. The tuning criterion is defined as the one aimed at identifying the controller gains through exhaustive search processes, with the goal of achieving the lowest possible value of the ϕ coefficient, representing the best performance.

Table 2 summarizes the results of the exhaustive searches and response indicators for all the operating modes when a 5% of the hydro power supplied step is imposed, comparing as well this results with the simulations considering Paynter's criterion. Note that none of the gains obtained are at the limits of the range of the exhaustive search, which guarantees that the point with the best ϕ value is within the range. In addition, Fig. 5 shows graphically the comparison, for each mode of operation, of the ϕ parameter, depending on whether the controller gains have been obtained according to Paynter's recommendation or the proposed mode-dependent tuning strategy.

TABLE 2. Governor setting and simulation results for each operating mode considering proposed mode-dependent tuning.

Operating mode	Criterion	K_p	K_i	NADIR (Hz)	t_s (s)	ϕ
1	Paynter	2.09	0.32	58.5831	47.60	0.8125
	Proposed	1.40	0.20	58.4449	16.70	0.0857
2	Paynter	1.57	0.24	58.6445	17.40	0.2967
	Proposed	1.60	0.26	58.6573	15.00	0.2557
3	Paynter	1.05	0.16	58.5784	38.60	0.6589
	Proposed	2.00	0.38	58.9093	12.10	0.2054
4	Paynter	1.05	0.16	58.5637	38.40	0.6557
	Proposed	2.00	0.38	58.5910	11.20	0.1902
5	Paynter	1.05	0.16	58.5834	38.70	0.6606
	Proposed	2.10	0.41	58.9384	10.40	0.1765
6	Paynter	0.52	0.08	58.1750	61.20	1.0520
	Proposed	2.20	0.41	59.0952	14.80	0.2504
7	Paynter	0.52	0.08	58.1822	61.30	1.0536
	Proposed	2.20	0.41	59.1068	14.80	0.2504

As can be seen from Table 2 and Fig. 5, the ϕ parameter improves in all modes of operation if the controller gains are obtained according to the proposed methodology with respect to the Paynter criterion, reducing to approximately 75% in the case of operating modes 6 and 7. With respect to the NADIR, except in operating mode 1 where there is a 138 mHz deterioration in the result obtained with the proposed criterion with respect to that obtained with Paynter, in all the other operating modes there is an improvement, increasing by 92 mHz in operating modes 6 and 7. In terms of frequency settling time, an improvement is obtained in all modes of operation due to the proposed criterion, varying from 2.4 s in mode 2 to 46.5 s in modes 6 and 7.

D. GOVERNOR GAINS SETTING FOR ALL OPERATING MODE: MODE-INDEPENDENT TUNING

For this controller tuning strategy, a mode-independent (permanent) tuning of the power plant governor is proposed. The possibility of using a fixed set of controller gains for all operating conditions is advantageous for plant operators, as modifying the gains based on the current mode may add complexity to the control process. Therefore, a compromise solution is obtained by selecting a pair of coefficients, K_p and K_i, from the first method that provides the best combined performance across all operating modes. The methodology proposed in this case is to obtain the average ϕ matrix for each combination of K_p and K_i, whose elements, one by one, are calculated as shown in (9), and select the one with the lowest value (analogous to the above), identifying the corresponding combination of K_p andK_i values.

$$\phi_{ave} = \frac{1}{n} \sum \phi(K_p, K_i) \tag{9}$$

where $n = 7$ as there are 7 operating modes. Although this is not the optimal point, it will be feasible for operation in any situation. Following this methodology, the obtained values for the controller gains are $K_p = 1.60$ and $K_i = 0.26$, that are identical to those obtained for mode 2. However, this fact is a coincidence. Table 3 shows a summary of the results obtained through this proposed compromise adjustment (mode-independent tuning) obtained for each operating configuration of the plant, in addition to the percent variation ($\%\Delta$) of the mode-independent tuning with respect to the adjustment itself for each operating mode. As can be observed and inferred, in all modes of operation—except for Mode 2, since the controller gains remain unchanged—the value of the proposed coefficient, ϕ, increases, that is, it worsens. This is mainly due to the increase in the settling time, as the variation in the NADIR value is minimal regardless of the mode of operation. Likewise, it can be observed in Fig. 5 that the values of ϕ obtained using the proposed mode-independent tuning criterion continue to improve compared to those obtained using the Paynter criterion as the tuning reference.

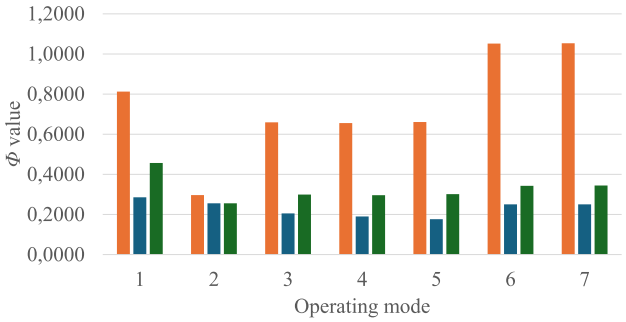

FIGURE 5. Comparison of ϕ value for the different operating modes assuming the Paynter's criterion (orange bars), the proposed mode-dependent tuning criterion (blue bars) and mode-independent tuning (green bars).

Likewise, Fig. 6 shows the dynamic response of the plant power output and the system frequency to a 5% step change in generation (due either to a sudden generation drop or an instantaneous generation increase) with respect to the initial power level. As can be seen, the PI controller tuned according to the Paynter criterion is significantly less aggressive, resulting in a smaller overshoot in generated power. However, due to this conservative behavior, the frequency reaches undesirably low values, dropping below 59 Hz. Regarding the two proposed criteria, results with mode-dependent tuning criterion clearly provides a slightly faster plant response. Nevertheless, the mode-independent tuning criterion still delivers fully acceptable results, while also outperforming those obtained using the Paynter tuning approach.

IV. RESULTS

To evaluate the effectiveness of the proposed adjustments, a series of 3,500 second simulations have been carried out to analyse the integration of wind energy in the

TABLE 3. Governor setting for all operating mode considering mode-independent tuning, ie. $K_P = 1.60$ and $K_i = 0.26$.

Operating mode	NADIR		t_s		ϕ	
	(Hz)	$\%\Delta$	(s)	$\%\Delta$	-	$\%\Delta$
1	58.4995	0.09	26.70	59.88	0.4564	59.75
2	58.6573	0	15.00	0	0.2557	0
3	58.7963	-0.19	17.60	45.45	0.2993	45.72
4	58.7796	-0.19	17.40	55.36	0.2960	55.63
5	58.8018	-0.23	17.70	70.19	0.3010	70.54
6	58.9285	-0.28	20.20	36.49	0.3428	36.90
7	58.9391	-0.28	20.30	37.16	0.3444	37.54

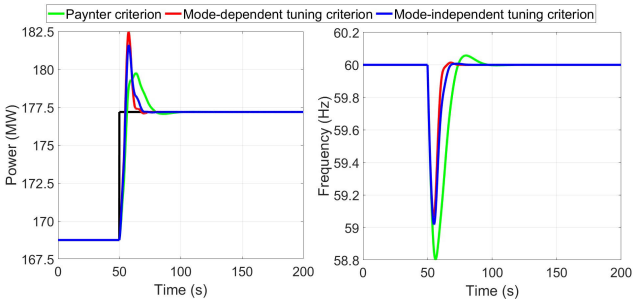

FIGURE 6. Dynamic response of the power plant due to a power demand step (solid black line): supplied power on the left and system frequency on the right, considering the different criteria proposed for operating mode 4.

proposed isolated power system, considering different levels of wind power. Initially, an installed power of 16.5 MW was assumed, analogous to the Villonaco wind farm (Loja, Ecuador), the first to be commissioned in the Ecuadorian electricity system [48]. The wind power penetration has been simulated using a representative power output profile for this technology, which is shown in Fig. 7 in p.u. units with respect to the wind power penetration power, without explicitly modeling any specific wind farm layout, following the approach previously suggested in [39]. In addition, greater wind farm capacity has been taken into account, in line with the country's commitment to increasing the penetration of renewable energies [32]. Specifically, scenarios have been considered in which the installed wind power capacity is scaled, reaching total installed capacities of 82.5 MW and 165 MW. These capacities correspond to multiplying the wind farm capacity of Villonaco by a factor of 5 and by a factor of 10, respectively.

To evaluate the effectiveness of the proposed criteria, several indicators have been used, including the maximum and minimum frequency values—namely, the frequency NADIR and CENIT, the frequency Mean Squared Error (MSE), which represents overall frequency stability—as well as the duration (t_{150}) during which the system frequency remains outside the limits established by the Ecuadorian system operator (± 150 mHz) [47]. Additionally, the control effort of the turbine nozzle has been assessed, quantified as the cumulative sum of actuator movements ($\int \Delta z$). For all indicators, the percentage variation ($\%\Delta$) has been calculated relative to the baseline scenario in which the power plant is adjusted according to the Paynter criterion [43].

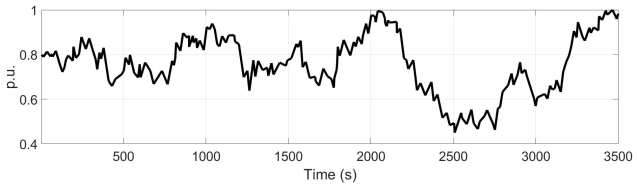

FIGURE 7. Wind power injected into the power system in p.u. values.

Table 4 summarizes the simulation results of the dynamic response of the Coca Codo Sinclair hydropower plant under different operating configurations, considering wind power variability and applying the proposed mode-dependent tuning criterion.

Regarding frequency response, operating modes 2 through 7 exhibit moderate improvements in both NADIR and CENIT values. Higher NADIR values indicate reduced underfrequency events, while lower CENIT values reflect a more limited frequency overshoot. Mode 6 shows the highest improvement in NADIR (+0.4122%), and Mode 1 is the only configuration that worsens both metrics simultaneously, with a reduction in NADIR (-0.0312%) and an increment in CENIT (+0.0231%). It is important to note that the controller gains were derived from simulations using a power step input, where the proposed tuning showed improved performance compared to Paynter's method. However, this improvement may not be maintained when subject to a wind power signal, as is the case in Operating mode 1.

Concerning MSE, all modes except Mode 1 show reductions with respect to the reference. Mode 1 yields a 146.36% increase in MSE, indicating a worse frequency regulation performance. Modes 6 and 7 achieve the largest improvements, reducing the MSE by over 96%, although their frequency excursions exceed system limits, as evidenced by poor CENIT and t_{150} metrics.

Regarding the t_{150} parameter, Modes 1 through 5 maintain this value at zero, ensuring full compliance with regulatory thresholds. In contrast, Modes 6 and 7 report a t_{150} of 1.90 s, representing 0.05% of the simulation time. The reduction in system inertia, which depends on the number of active generating units, explains the increased frequency variations observed in NADIR, CENIT and t_{150} values. With all four units running in Operating Mode 1, inertia is at its maximum. In contrast, when only one turbine is active, inertia drops to 25%, amplifying the system's sensitivity to power fluctuations. This phenomenon will be seen in the rest of the simulations, regardless of the adjustment methodology.

Finally, the distributor effort, represented by $\int \Delta z$, is reduced by 13.17% in Mode 1 relative to the classical controller due to the fact, as previously explained, that the proposed setting causes the controller to be more energetic, thus producing more turbine nozzle movements. Modes 3 to 5 increase this mechanical effort by 17–18%, while Modes 6 and 7 show the largest increases, exceeding 44%. This phenomenon is attributed to the tuning of the controller itself, which results in a more aggressive behavior compared to that proposed by Paynter. Regarding the improvement across different operating modes, the enhancement is less significant in those with a greater number of units running, since Paynter's tuning is designed for nominal operating conditions, but not for scenarios with lower generated power. This confirms the need to analyze the various operating modes considered in the article.

Therefore, this tuning improves the system frequency regulation at the expense of increased nozzle activity, which leads to greater wear and must be considered in the power plant's maintenance planning.

TABLE 4. Simulation results using variable wind speeds assuming the mode-dependent tuning criterion (gains values in Table 2) and 16.5 MW wind power penetration scenario.

Operating mode	NADIR		CENIT		MSE		t_{150}		$\int \Delta z$	
	Hz	%Δ	Hz	%Δ	$10^{-4}Hz^2$	%Δ	s	%Δ	p.u.	%Δ
1	59.939	-0.0312	60.071	0.0231	9.45	146.36	0	-	0.2037	-13.17
2	59.935	0.0036	60.079	-0.0037	9.75	-14.63	0	-	0.2678	1.984
3	59.933	0.0995	60.092	-0.0867	10.30	-81.49	0	-	0.3985	17.15
4	59.933	0.1005	60.093	-0.0861	10.41	-81.46	0	-	0.4024	17.38
5	59.938	0.1073	60.088	-0.0921	8.91	-84.00	0	-	0.4009	18.21
6	58.881	0.4122	60.158	-0.4707	35.01	-96.17	1.90	-99.72	0.7500	44.96
7	58.881	0.4106	60.156	-3.4705	34.91	-96.18	1.90	-99.75	0.7452	44.56

On the other hand, Table 5 presents the simulation results considering the same wind power, but using mode-independent tuning strategy to set the controller gains. Similar to the case of the power step simulation developed in the previous section, it is observed that the results generally improve (except in operating mode 1) compared to the tuning proposed by Paynter, although not to the same extent as with an mode-dependent tuning criterion. Thus, improvements in the case of frequency oscillations range from 0.0039% of the NADIR in mode 2 to 0.3951% at the CENIT in mode 7.

Regarding the MSE, except for the 47% deterioration in mode 1, an improvement is observed in the rest of the operating modes, with the highest being in mode 7, which reaches 90.712%. Again, this improvement is even greater in the case of mode-dependent tuning criterion. Concerning the (t_{150}) parameter, modes 1 to 5 maintain this value at zero, while modes 6 and 7 yield a t_{150} value close to 13 seconds, representing 0.37% of the simulation time. Finally, the distributor effort shows an increase, as expected, ranging from 1.99% to 37% (except in mode 1) because this controller adjustment makes it more aggressive, thus requiring greater effort from the plant. Again, this effort is lower than if the plant were adjusted with the proposed mode-dependent tuning criterion.

Overall, the results show that the plant can be operated with a single tuning that does not depend on the operating mode, simplifying its operation and improving, in most cases, the results obtained with the classical tuning proposed by Paynter, which, in turn, depends on the operating mode.

Graphically, a part of the simulation for one of the operating modes, specifically mode 5, is shown in Fig. 8, where both the power generated by the plant and the system frequency are represented. In this figure, it is evident that

TABLE 5. Simulation results using variable wind speeds assuming the mode-independent tuning criterion (i.e., $K_p = 1.60$ and $K_i = 0.26$) and 16.5 MW wind power penetration scenario.

Operating	NADIR		CENIT		MSE		t_{150}		$\int \Delta z$	
mode	Hz	%Δ	Hz	%Δ	$10^{-7} Hz^2$	%Δ	s	%Δ	p.u.	%Δ
1	59.947	-0.0186	60.065	0.0136	5.65	47.106	0	-	0.2183	-6.93
2	59.935	0.0036	60.079	-0.0037	9.75	-14.628	0	-	0.2678	1.984
3	59.909	0.0607	60.110	-0.0582	21.51	-61.356	0	-	0.3756	10.42
4	59.909	0.0611	60.110	-0.0579	21.61	-61.325	0	-	0.3790	10.55
5	59.910	0.0605	60.110	-0.0583	21.51	-61.366	0	-	0.3744	10.39
6	58.828	0.3231	60.203	-0.3955	85.01	-90.7066	13.15	-98.07	0.7089	37.01
7	58.829	0.3225	60.202	-0.3951	84.81	-90.712	12.80	-98.11	0.7046	36.69

the mode-dependent tuning criterion, marked in blue, significantly improves the frequency deviations, although at the cost of higher excursions in the power generated by the plant, compared to those produced with Paynter tuning, marked in black. Furthermore, the mode-independent tuning criterion, also marked in blue, produces an intermediate response, thereby improving the results obtained with Paynter's tuning as well.

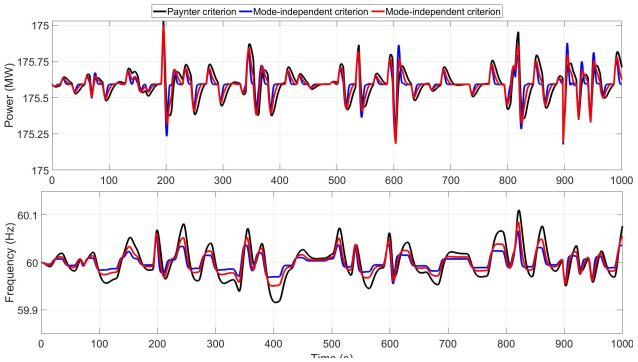

FIGURE 8. Dynamic response of hydropower plant power and system frequency with Paynter, mode-dependent and mode-independent tuning criteria for operating mode 5 with a 16.5 MW wind power penetration.

Table 6 presents the simulation results for the dynamic frequency response of the Coca Codo Sinclair hydropower plant under different operating modes, using the proposed mode-dependent tuning strategy in a scenario with 82.5 MW of wind power penetration. With increased wind penetration, the overall system dynamics become more demanding, particularly in terms of maintaining frequency stability. Regarding NADIR, the worst value is obtained with mode 6 operation, reaching 59.405 Hz, although this is a fully acceptable value. Modes 2 to 7 improve upon the Paynter's reference, with Mode 7 achieving the highest gain (+2.0829%). In contrast, Mode 1 slightly worsens the NADIR (–0.1564%). For the CENIT, the analysis is very similar to that of NADIR: mode of operation 1 worsens slightly compared to the Paynter benchmark, while all other modes improve, reaching improvements of up to 2.26% for mode of operation 6.

The MSE follows the same pattern observed at 16.5 MW wind penetration. Mode 1 again shows a substantial degradation (+146.44%), however, the MSE value for this operation mode is one of the lowest of all modes of operation. All other modes improve the MSE significantly, particularly Modes 6 and 7 (–96.16% and –96.18%, respectively), as in the lower wind penetration scenario.

In terms of t_{150}, the impact of higher wind penetration becomes evident. Unlike the previous scenario (where Modes 1–5 maintained $t_{150} = 0$), here all modes show nonzero values. Modes 1, 2 and 5 yield the lowest t_{150} (222-274 s), reducing it by over 75% compared to the reference. Mode 1, however, leads to a massive increase (+481.41%), although the time that the frequency is outside the TSO recommendation, t_{150}, is around 6% of the simulation time.

Regarding actuator effort ($\int \Delta z$), Mode 1 again stands out for reducing it by 13.26%, consistent with the 13.17% reduction observed at 16.5 MW. Modes 2 to 7 show increased mechanical effort (2–45%), while clearly due to the fact that the controller is much more energetic to better dampen oscillations due to high wind energy penetration.

TABLE 6. Simulation results assuming the proposed mode-dependent criterion (gains values in Table 2) using variable wind power and a scenario of 82.50 MW wind power penetration.

Operating	NADIR		CENIT		MSE		t_{150}		$\int \Delta z$	
mode	Hz	%Δ	Hz	%Δ	$10^{-5} Hz^2$	%Δ	s	%Δ	p.u.	%Δ
1	59.695	-0.1564	60.352	0.1152	2.36	146.44	222.42	481.41	1.0188	-13.26
2	59.676	0.0179	60.393	-0.0185	2.44	-14.63	265.80	-10.07	1.3391	1.99
3	59.662	0.5030	60.460	-0.4286	2.58	-81.48	323.36	-75.60	1.9932	17.24
4	59.660	0.5082	60.466	-0.4257	2.59	-81.45	330.38	-75.29	2.0129	17.47
5	59.688	0.5423	60.442	-0.4552	2.22	-84.00	274.10	-79.24	2.0054	18.31
6	59.405	2.0916	60.788	-2.2604	8.74	-96.16	956.86	-65.46	3.7498	45.66
7	59.407	2.0829	60.781	-2.2598	8.71	-96.17	948.94	-65.73	3.7257	45.26

Under the mode-independent tuning with 82.50 MW of wind power penetration, whose results are listed in Table 7, the system exhibits intermediate performance between the mode-dependent tunings and the classical Paynter controller. Mode 1 offers a MSE increment (+47.16%) compared to Paynter's setting, similar to it slightly worsens NADIR (–0.0936%) and CENIT (+0.0680%). Modes 2 to 7 exhibit similar improvements (although inferior) to their mode-dependent setting, with consistent reductions in MSE (up to –61%) and noticeable improvements in frequency extremes—both higher NADIR and lower CENIT—indicating enhanced frequency stability.

TABLE 7. Simulation results assuming mode-independent setting criterion (i.e., $K_p = 1.60$ and $K_i = 0.26$) using variable wind power outputs and a scenario of 82.50 MW wind power penetration.

Operating	NADIR		CENIT		MSE		t_{150}		$\int \Delta z$	
mode	Hz	%Δ	Hz	%Δ	$10^{-5} Hz^2$	%Δ	s	%Δ	p.u.	%Δ
1	59.733	-0.0936	60.324	0.0680	1.41	47.161	103.77	171.25	1.0922	-7.00
2	59.677	0.0179	60.393	-0.0185	2.44	-14.628	265.80	- 10.07	1.3391	1.99
3	59.546	0.3068	60.545	-0.2876	5.38	-61.339	587.54	- 55.67	1.8782	10.48
4	59.542	0.3091	60.551	-0.2857	5.40	-61.309	597.45	- 55.32	1.8952	10.60
5	59.547	0.3060	60.543	-0.2880	5.36	-61.349	582.40	- 55.89	1.8719	10.44
6	59.138	1.6338	61.015	-1.8957	21.20	-90.676	1719.36	-37.94	3.5427	37.62
7	59.144	1.6304	61.008	-0.8942	21.20	-90.682	1712.83	-38.14	3.5213	37.29

Graphically, part of the simulation for one of the operating modes, specifically mode 4, is shown in Fig. 9, where both the power generated by the plant and the system frequency are represented. In this figure, it is again evident that the mode-dependent tuning significantly improves the frequency deviations at the cost of greater excursions in the power

generated by the plant, compared to those produced with Paynter's tuning. Given the higher penetration of wind energy, in this case, the limits of ±150 mHz recommended by the system operator are exceeded. However, the graphical results confirm the analysis from Tables 6 and 7, i.e., it is observed that the system frequency simulated with Paynter's tuning exceeds these limits for a longer duration. Finally, the mode-independent tuning is again shown to produce an intermediate response, thereby improving the results obtained with Paynter's tuning as well.

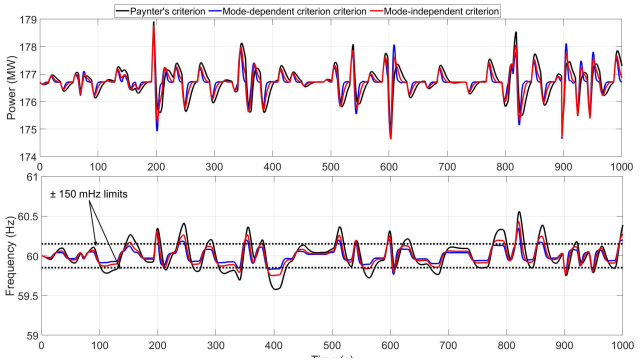

FIGURE 9. System frequency and hydropower plant power dynamics under Paynter, mode-dependent, and mode-independent tuning criteria, evaluated for operating mode 4 with 82.5 MW wind power penetration.

When wind power penetration is significantly higher than in the previous scenarios—such as the case of 165 MW—the adverse effects on power quality become evident, as can be inferred from the results shown in Table 8, obtained using the mode-dependent tuning, and those in Table 8, corresponding to the mode-independent tuning. As in the previous simulations, the results are better when the controller is tuned using the mode-dependent strategy rather than the mode-independent one.

TABLE 8. Simulation results assuming the proposed mode-dependent criterion (gains values in Table 2) using variable wind power and a scenario of 165 MW wind power penetration.

Operating	NADIR		CENIT		MSE		t_{150}		$\int \Delta z$	
mode	Hz	%Δ	Hz	%Δ	$10^{-5}Hz^2$	%Δ	s	%Δ	p.u.	%Δ
1	59.391	-0.3142	60.703	0.2292	9.43	146.54	1050.0	109.81	2.0383	-13.42
2	59.353	0.0361	60.785	-0.0367	9.73	-14.62	1130.9	-8.56	2.6790	1.99
3	59.325	1.0197	60.918	-0.8448	10.3	-81.47	1222.3	-47.97	3.9880	17.36
4	59.320	1.0303	60.930	-0.8392	10.3	-81.44	1228.1	-47.89	4.0280	17.59
5	59.376	1.0993	60.882	-0.8975	8.87	-83.99	1043.4	-55.53	4.0125	18.44
6	58.810	4.2624	61.573	-4.2624	34.9	-96.14	2135.6	-31.72	7.4861	46.22
7	58.815	4.2434	61.559	-4.2434	34.8	-96.15	2129.2	-31.87	7.4403	45.87

TABLE 9. Simulation results assuming mode-dependent criterion (i.e., $K_p = 1.60$ and $K_i = 0.26$) using variable wind power outputs and a scenario of 165 MW wind power penetration.

Operating	NADIR		CENIT		MSE		t_{150}		$\int \Delta z$	
mode	Hz	%Δ	Hz	%Δ	$10^{-5}Hz^2$	%Δ	s	%Δ	p.u.	%Δ
1	59.466	-0.1881	60.647	0.1358	5.63	47.23	748.68	49.53	2.1859	-7.142
2	59.353	0.0361	60.785	-0.0367	9.73	-14.63	1130.9	-8.56	2.6790	1.993
3	59.092	0.6223	61.089	-0.5666	21.5	-61.32	1772.9	-24.53	3.7565	10.54
4	59.084	0.6273	61.099	-0.5630	21.5	-61.29	1782.1	-24.38	3.7906	10.66
5	59.095	0.6208	61.085	-0.5674	21.4	-61.39	1769.8	-24.56	3.7438	10.51
6	58.276	3.3150	62.025	-3.6035	84.7	-90.64	2607.1	-16.64	7.0811	38.31
7	58.286	3.3070	62.012	-3.6007	84.4	-90.64	2603.4	-16.70	7.0386	37.99

Nevertheless, under both controller tuning strategies, the system frequency reaches undesirable values. This is particularly evident in operating mode 6 with mode-independent tuning, where the NADIR reaches 58.276 Hz. It is straightforward to understand that poorer performance is expected in operating modes where only one unit is connected to the grid and generating electricity (i.e., modes 5, 6, and 7), compared to the case where all units are connected (i.e., mode 1). In fact, the NADIR in this latter case is 59.466 Hz, representing a difference of nearly 1200 mHz compared to mode 6. These differences are also observed in both the MSE and t_{150}, which increase compared to cases with lower wind power penetration, indicating a deterioration in system frequency quality. This quality improves with the number of operating units and, consequently, with the level of synchronous inertia in the system.

The increased regulatory demand caused by the high wind power penetration is also reflected in the greater effort required from electromechanical components, evaluated through $\int \Delta z$, which increases up to seven times compared to the situation with ten times lower wind power penetration.

An increase in wind power penetration can lead to unacceptable frequency fluctuations in the system. However, this does not preclude achieving high levels of wind integration; rather, it highlights the need to adapt both the operating mode of the power plant and the power system. The improved results observed in Operating Mode 1 are not due to higher electrical power generation, but to the fact that four generating units remain online, providing greater system inertia, which naturally helps to dampen frequency fluctuations. Nevertheless, it is not necessary for all four units to be generating electricity; they could operate as synchronous condensers, contributing inertia only. Additionally, the installation of fast-response storage systems—such as batteries, flywheels, or supercapacitors—could be considered. The evaluation of these systems constitutes the future line of research for this team.

V. CONCLUSION

This paper has presented a methodology for tuning the speed governor gains of the Coca Codo Sinclair Hydropower Plant to enable its operation in isolated mode, representing one of the most demanding scenarios for frequency regulation. The proposed approach is based on the definition of a performance penalty index, which quantifies the plant's response to a step change in generated power. This index is minimized through an exhaustive search over the controller gain space. A detailed dynamic model has been developed in the Matlab Simulink environment, incorporating the complex hydraulic circuit of the plant, including long conduits and the coupling between generating units, a configuration rarely addressed in the literature.

Two tuning strategies have been proposed: one dependent on the operating mode, i.e., the number and combination of generating units online, and another mode-independent strategy, which applies fixed gains regardless of the

operational configuration. Several simulation scenarios have been performed to evaluate the ability of the hydropower plant to damp frequency fluctuations caused by variations in wind power, considering expansion plans for renewable energy in Ecuador and the decarbonization of Amazonian provinces currently served by thermal generation.

The proposed tuning strategies were evaluated using electrical performance metrics and indicators of mechanical stress on turbine components, and were compared with a conventional tuning method. The results show a clear improvement in frequency quality under both strategies, particularly when the gains are adapted to the operating mode. However, while the mode-independent strategy also yields improvements, it leads to more aggressive controller action, increasing mechanical wear. These findings highlight the importance of considering system inertia and generator configuration when integrating high levels of wind energy. Future work will explore operational strategies aimed at increasing wind power penetration while maintaining system reliability and minimizing equipment wear. These findings not only validate the effectiveness of the proposed methodology in improving frequency regulation, but also demonstrate its relevance for systems with long penstocks operating in isolation, a context where traditional tuning approaches often fall short. By explicitly accounting for hydraulic interactions and generator configurations, the methodology contributes to more realistic and robust controller design. Moreover, it supports the broader objective of increasing wind power penetration while preserving system reliability and minimizing mechanical degradation.

NOMENCLATURE

The following nomenclature has been used:

a_w	m/s	Wave speed.
A_t		Turbine parameter.
D_t		Turbine parameter.
f	p.u.	System frequency.
g	m/s^2	Gravity acceleration.
H_b	m	Base head.
h_i	p.u.	Net head of the i-th turbine.
h_m	p.u.	Head at the end of the m-th Γ element of the penstock.
$\int \Delta z$	p.u.	Average hydro-power generation units' wear.
K_i		Integral gain in hydro PI governor control.
K_p		Proportional gain in hydro PI governor control.
L	m	Penstock length.
$2H_{h,i}$	s	Inertia constant of each i on-line hydro unit.
n_t		Number of segments in which the penstock is divided.
p_{dem}	p.u.	Constant power demand by consumers.
$p_{h,i}$	p.u.	Power supplied by each i on-line hydro unit.
p_w	p.u.	Power supplied by the wind farms.
Q_b	m^3/s	Base flow.
q_i	p.u.	Flow through the i-th turbine.
q_{nl}	p.u.	No-load flow in the turbine.
$q_{p,m}$	p.u.	Flow at the end of the m-th Γ element of the penstock.
$\frac{r}{2}$	p.u.	Continuous head losses coefficient in the penstock.
S	m^2	Penstock section.
t_{150}	s	Time during which the frequency is outside the ± 150 mHz limit.
t_s	s	Frequency settling time.
T_e	s	Water elastic time (L/a_w).
T_w	s	Water starting time.
ϕ		Defined coefficient to obtain controller gains.
z_i	p.u.	Nozzle opening of i-th turbine.
MSE		Frequency mean square error.
PID		Proportional - Integral - Derivative control.

REFERENCES

[1] Q. Hassan, P. Viktor, T. J. Al-Musawi, B. M. Ali, S. Algburi, H. M. Alzoubi, A. K. Al-Jiboory, A. Z. Sameen, H. M. Salman, and M. Jaszczur, "The renewable energy role in the global energy transformations," *Renew. Energy Focus*, vol. 48, Mar. 2024, Art. no. 100545.

[2] X. Liang, "Emerging power quality challenges due to integration of renewable energy sources," *IEEE Trans. Ind. Appl.*, vol. 53, no. 2, pp. 855–866, Mar. 2017.

[3] O. Erdinc, N. G. Paterakis, and J. P. S. Catalão, "Overview of insular power systems under increasing penetration of renewable energy sources: Opportunities and challenges," *Renew. Sustain. Energy Rev.*, vol. 52, pp. 333–346, Dec. 2015.

[4] B. Mohandes, M. S. E. Moursi, N. Hatziargyriou, and S. E. Khatib, "A review of power system flexibility with high penetration of renewables," *IEEE Trans. Power Syst.*, vol. 34, no. 4, pp. 3140–3155, Jul. 2019.

[5] M. Valavi and A. Nysveen, "Variable-speed operation of hydropower plants: A look at the past, present, and future," *IEEE Ind. Appl. Mag.*, vol. 24, no. 5, pp. 18–27, Sep. 2018.

[6] W. Yang, J. Yang, W. Guo, and P. Norrlund, "Response time for primary frequency control of hydroelectric generating unit," *Int. J. Electr. Power Energy Syst.*, vol. 74, pp. 16–24, Jan. 2016.

[7] J. Zou, M. Pipattanasomporn, S. Rahman, and X. Lai, "A frequency regulation framework for hydro plants to mitigate wind penetration challenges," *IEEE Trans. Sustain. Energy*, vol. 7, no. 4, pp. 1583–1591, Oct. 2016.

[8] S. Cassano and F. Sossan, "Stress-informed control of medium-and high-head hydropower plants to reduce penstock fatigue," *Sustain. Energy, Grids Netw.*, vol. 31, Sep. 2022, Art. no. 100688.

[9] E. J. Oliveira, L. M. Honório, A. H. Anzai, L. W. Oliveira, and E. B. Costa, "Optimal transient droop compensator and PID tuning for load frequency control in hydro power systems," *Int. J. Electr. Power Energy Syst.*, vol. 68, pp. 345–355, Jun. 2015.

[10] M. R. Basir Khan, J. Pasupuleti, and R. Jidin, "Load frequency control for mini-hydropower system: A new approach based on self-tuning fuzzy proportional-derivative scheme," *Sustain. Energy Technol. Assessments*, vol. 30, pp. 253–262, Dec. 2018.

[11] J.-W. Perng, Y.-C. Kuo, and K.-C. Lu, "Design of the PID controller for hydro-turbines based on optimization algorithms," *Int. J. Control, Autom. Syst.*, vol. 18, no. 7, pp. 1758–1770, Jul. 2020.

[12] M. Joshi, G. Sharma, and E. Çelik, "Load frequency control of hydro-hydro power system using Fuzzy-PSO-PID with application of UC and RFB," *Electr. Power Compon. Syst.*, vol. 51, no. 12, pp. 1156–1170, Jul. 2023.
[13] D. Trong Tran, A.-T. Tran, V. van Huynh, and T. Duc do, "Decentralized frequency regulation by using novel PID sliding mode structure in multi-area power systems with hydropower turbines," *IEEE Access*, vol. 13, pp. 18850–18862, 2025.
[14] F. Qu and W. Guo, "Coupling transient behavior of primary frequency regulation of hydropower plant," *Sustain. Energy Technol. Assessments*, vol. 52, Aug. 2022, Art. no. 102227.
[15] Working Group Prime Mover and Energy Supply, "Hydraulic turbine and turbine control models for system dynamic studies," *IEEE Trans. Power Syst.*, vol. 7, no. 1, pp. 167–179, Feb. 1992.
[16] O. H. Souza, N. Barbieri, and A. H. M. Santos, "Study of hydraulic transients in hydropower plants through simulation of nonlinear model of penstock and hydraulic turbine model," *IEEE Trans. Power Syst.*, vol. 14, no. 4, pp. 1269–1272, Dec. 1999.
[17] X. Liu and C. Liu, "Eigenanalysis of oscillatory instability of a hydropower plant including water conduit dynamics," *IEEE Trans. Power Syst.*, vol. 22, no. 2, pp. 675–681, May 2007.
[18] C. Nicolet, B. Greiveldinger, J. J. Herou, B. Kawkabani, P. Allenbach, J.-J. Simond, and F. Avellan, "High-order modeling of hydraulic power plant in islanded power network," *IEEE Trans. Power Syst.*, vol. 22, no. 4, pp. 1870–1880, Nov. 2007.
[19] K. A. Naik, P. Srikanth, and P. Negi, "Imc tuned pid governor controller for hydro power plant with water hammer effect," *Proc. Technol.*, vol. 4, pp. 845–853, Jan. 2012.
[20] W. Guo, J. Yang, J. Chen, and Y. Teng, "Effect mechanism of penstock on stability and regulation quality of turbine regulating system," *Math. Problems Eng.*, vol. 2014, no. 1, Jan. 2014, Art. no. 349086.
[21] G. Martínez-Lucas, J. I. Sarasúa, J. Á. Sánchez-Fernández, and J. R. Wilhelmi, "Power-frequency control of hydropower plants with long penstocks in isolated systems with wind generation," *Renew. Energy*, vol. 83, pp. 245–255, Nov. 2015.
[22] J. I. Sarasúa, J. I. Pérez-Díaz, J. R. Wilhelmi, and J. Á. Sánchez-Fernández, "Dynamic response and governor tuning of a long penstock pumped-storage hydropower plant equipped with a pump-turbine and a doubly fed induction generator," *Energy Convers. Manage.*, vol. 106, pp. 151–164, Dec. 2015.
[23] R. Tang, J. Yang, and W. Yang, "Stability of frequency regulation of pumped-storage plants with multiple units sharing common penstock and busbar," *IOP Conf. Ser., Earth Environ. Sci.*, vol. 163, Jul. 2018, Art. no. 012094, doi: 10.1088/1755-1315/163/1/012094.
[24] R. Kumari, K. Desingu, T. R. Chelliah, and S. V. A. Sharma, "Development trends and future prospects of hydro-turbine control systems," in *Proc. IEEE Ind. Appl. Soc. Annu. Meeting*, Sep. 2019, pp. 1–10.
[25] S. Cassano, C. Nicolet, and F. Sossan, "Reduction of penstock fatigue in a medium-head hydropower plant providing primary frequency control," in *Proc. 55th Int. Universities Power Eng. Conf. (UPEC)*, Sep. 2020, pp. 1–6.
[26] G. Li, J. Zhang, X. Wu, and X. Yu, "Small-signal stability and dynamic behaviors of a hydropower plant with an upstream surge tank using different PID parameters," *IEEE Access*, vol. 9, pp. 104837–104845, 2021.
[27] A. Heidari-Akhijahani and K. L. Butler-Purry, "A review on black-start service restoration of active distribution systems and microgrids," *Energies*, vol. 17, no. 1, p. 100, Dec. 2023. [Online]. Available: https://www.mdpi.com/1996-1073/17/1/100
[28] F. Logic. (2024). *Why Portable Diesel Generators Are Vital for Remote Worksites*. Accessed: May 11, 2025. [Online]. Available: https://www.fuellogic.net/why-portable-diesel-generators-are-vital-for-remote-worksites/
[29] M. A. Hossain, A. S. M. A. Hossain, and M. A. H. Chowdhury, "Techno-economic analysis of off-grid PV-diesel power generation system for rural electrification in sub-Saharan Africa," *Renew. Sustain. Energy Rev.*, vol. 124, Feb. 2020, Art. no. 109792. [Online]. Available: https://www.sciencedirect.com/science/article/pii/S0960148122019085
[30] (2023). *Atlas del Sector Eléctrico Ecuatoriano 2023*. Agencia de Regulacióny Control de Energía y Recursos Naturales no Renovables (ARCERNNR), Quito, Ecuador. Accessed: May 8, 2025. [Online]. Available: https://controlelectrico.gob.ec/wpcontent/uploads/downloads/2024/07/Atlas-del-Sector-Electrico-Ecuatoriano-2023.pdf
[31] (2023). *Plan Maestro de Electricidad*. Corporación Eléctrica del Ecuador (CELEC EP), Quito, Ecuador. Accessed: May 8, 2025. [Online]. Available: https://www.celec.gob.ec/wpcontent/uploads/2023/02/Plan-Maestro-de-Electricidad.pdf
[32] Ministerio de Electricidad y Energía Renovable (MEER). (2013). *Atlas Eólico del Ecuador*. Quito, Ecuador. Accessed: May 8, 2025. [Online]. Available: https://pdfcoffee.com/atlas-eolico-ecuador-meer-2013-pdf-4-pdf-free.html
[33] *Plan Nacional de Desarrollo Energético*, SENPLADES, Quito, Ecuador, 2019.
[34] M. de Energía y Minas, "Informe de Energía y Desarrollo Sostenible en Ecuador," Insituto de Investigación Geológico y Energético (IIGE), Quito, Ecuador, Ministerio de Energía y Recursos Naturales No Renovables. 2018.
[35] M. Cordero, S. Pórez, and J. Castillo, "Hydraulic system design of the coca codo sinclair hydroelectric power plant," *J. Hydraulic Eng.*, vol. 142, no. 5, 2016, Art. no. 04016035.
[36] J. Ochoa, R. López, and P. Ramírez, "Optimization of penstock design for large hydroelectric plants: Coca Codo Sinclair case study," *Renew. Energy*, vol. 105, pp. 123–134, Jan. 2017.
[37] D. Salazar, R. Acosta, and L. Méndez, "Performance of Pelton turbines in high-head hydropower plants: A case study of coca codo sinclair," *Energy*, vol. 152, pp. 1044–1054, Jan. 2018.
[38] M. Pezic and V. M. Cedrés, "Unit commitment in fully renewable, hydro-wind energy systems," in *Proc. 10th Int. Conf. Eur. Energy Market (EEM)*, May 2013, pp. 1–8.
[39] G. Martínez-Lucas, J. I. Sarasúa, J. Á. Sánchez-Fernández, and J. R. Wilhelmi, "Frequency control support of a wind-solar isolated system by a hydropower plant with long tail-race tunnel," *Renew. Energy*, vol. 90, pp. 362–376, May 2016.
[40] S. P. Mansoor, D. I. Jones, D. A. Bradley, F. C. Aris, and G. R. Jones, "Reproducing oscillatory behaviour of a hydroelectric power station by computer simulation," *Control Eng. Pract.*, vol. 8, no. 11, pp. 1261–1272, Nov. 2000.
[41] M. H. Chaudhry, *Applied Hydraulic Transients* 1979. [Online]. Available: https://link.springer.com/book/10.1007/978-1-4614-8538-4
[42] G. Martínez-Lucas, J. I. Pérez-Díaz, M. Chazarra, J. I. Sarasúa, G. Cavazzini, G. Pavesi, and G. Ardizzon, "Risk of penstock fatigue in pumped-storage power plants operating with variable speed in pumping mode," *Renew. Energy*, vol. 133, pp. 636–646, Apr. 2019. [Online]. Available: https://www.sciencedirect.com/science/article/pii/S0960148118312448
[43] H. Paynter, *A Palimpsest on the Electronic Analogue Art*. Boston, MA, USA: Philbrik Researches Inc., 1955.
[44] G. Martínez-Lucas, J. I. Sarasúa, and J. Á. Sánchez-Fernández, "Eigen analysis of wind–hydro joint frequency regulation in an isolated power system," *Int. J. Electr. Power Energy Syst.*, vol. 103, pp. 511–524, Dec. 2018.
[45] *IEEE Guide for the Application of Turbine Governing Systems for Hydroelectric Generating Units—Redline*, Standard 1207-2011 (Revision to IEEE Std 1207-2004)-Redline, 2011, pp. 1–139.
[46] C. Seneviratne and C. Ozansoy, "Frequency response due to a large generator loss with the increasing penetration of wind/PV generation—A literature review," *Renew. Sustain. Energy Rev.*, vol. 57, pp. 659–668, May 2016.
[47] Agencia de Regulación y Control de Energía y Recursos Naturales No Renovables (ARCERNNR). (Jul. 2024). *Código de Operación del Sistema Eléctrico Ecuatoriano*. Resolución Nro. ARCERNNR-010/2024, Publicada en el Registro Oficial Nro. 622, el 15 de agosto de 2024. Regulación Nro. ARCERNNR-001/24. [Online]. Available: https://controlelectrico.gob.ec/wpcontent/uploads/downloads/2024/08/Reg-ARCERNNR-001-24.pdf
[48] Corporación Eléctrica del Ecuador (CELEC EP). (2023) *Central Eólica Villonaco. Consultado El 9 De Mayo De 2025*. [Online]. Available: https://www.celec.gob.ec/gensur/informacion-tecnica/centraleolica-villonaco/

GUILLERMO MARTÍNEZ-LUCAS was born in Madrid, Spain, in 1989. He received the M.Sc. degree in civil engineering, with a specialization in hydraulics and energy from the Technical University of Madrid (UPM), Madrid, in 2013, the B.A. degree in business administration and management from the National University of Distance Education (UNED), Madrid, in 2018, and the Ph.D. degree (cum laude) in civil engineering from UPM, in 2018. His doctoral dissertation, titled ''Frequency Control of Hybrid Wind-Hydro Power Plants With Long Conduits in Isolated Power Systems,'' received the distinction of Outstanding and international mention.

He joined the Department of Civil Engineering: Hydraulics, Energy and Environment, UPM, in 2016, first as an Assistant and then an Assistant Professor. Since 2022, he has been an Associate Professor with UPM. He has authored or co-authored more than 15 journal articles indexed in the Journal Citation Reports (JCR) and has presented his work at multiple international conferences. He has participated in five publicly funded research projects, eight industry-funded research contracts, and led an internally funded research project supported by Madrid Government. His research focuses on the control of hydroelectric and hybrid hydro-wind power systems, particularly in the context of isolated power networks.

Dr. Martínez-Lucas has been a member of the EERA Joint Program on Energy Storage, since 2016, and the EERA Joint Program on Hydropower, since 2019. He has received several academic distinctions and actively contributes to research and innovation in the field of renewable energy systems.

ANA FERNÁNDEZ-GUILLAMÓN was born in Spain, in 1994. She received the B.S. degree in electrical engineering, specializing in power plants and renewable energies from the University of Castilla–La Mancha (UCLM), Ciudad Real, Spain, in 2016, and the M.S. degree in renewable energies and the Ph.D. degree (cum laude) in renewable energies and energy efficiency from the Polytechnic University of Cartagena (UPCT), Cartagena, Spain, in 2017 and 2021, respectively.

She received a research initiation grant from the Department of Mathematics, UCLM, in 2015. She was an Internal Student in electronic technology with UPCT, from 2016 to 2017. In 2017, she received the National University Teaching Training Fellowship (FPU) to join the Department of Electrical Engineering, UPCT, where she carried out her doctoral research. She is currently an Interim Assistant Professor with the Department of Applied Mechanics and Project Engineering, UCLM. She is a member of the research group ''Energy Integration in the Grid,'' UCLM. She has completed three research stays at the Technical University of Denmark (DTU). She is supervising one Ph.D. student. She has authored or co-authored over 30 peer-reviewed journal articles and has participated in 20 international conferences, including one as an invited speaker. Her research interests include grid integration of renewable energy, energy efficiency, and ocean energy systems.

Dr. Fernández-Guillamón serves as a regular reviewer for IEEE, Elsevier, Springer, and MDPI journals, and has edited three special issues in international journals.

VICTOR A. GALLO MIER was born in Quito, Ecuador, in 1999. He received the B.S. degree (cum laude) in civil engineering from the Universidad San Francisco de Quito, Quito, Ecuador, in 2022, and the M.S. degree in civil engineering systems from the Universidad Politécnica de Madrid, Madrid, Spain, in 2024. His major field of study is civil engineering, with a focus on hydroelectric systems. His master's thesis, titled ''Modeling the Dynamic Behavior of the Coca Codo Sinclair Hydropower Plant Contributing to Grid Regulation in Ecuador,'' led to his involvement in research projects related to the control of hydro and hydro-wind power systems.

From 2021 to 2022, he was a Teaching Assistant with the Universidad San Francisco de Quito, supporting course planning and assessment in fluid mechanics, hydraulics, sanitary engineering, and construction management. Since 2022, he has been an Independent Contractor on large-scale civil works and sanitation and sewerage system projects. His current research interests include dynamic modeling and control strategies for renewable energy integration.

Mr. Gallo Mier is a member of various professional organizations in the fields of civil and environmental engineering. He has received academic honors for his undergraduate performance and is actively engaged in collaborative research initiatives.

JOSÉ IGNACIO SARASUA was born in Madrid, Spain, in June 1977. He received the M.Sc. and Ph.D. degrees in civil engineering from the Technical University of Madrid (UPM), Madrid, Spain, in 2001 and 2009, respectively. His major field of study was hydraulic and energy engineering.

He worked in several companies related to environmental engineering and taught at Universidad Alfonso X El Sabio. In 2011, he joined the Department of Hydraulic, Energy and Environmental Engineering, School of Civil Engineering, UPM, as a Non-Tenured Associate Professor. He has participated in various research and consulting projects for public and private companies in Spanish electric power sector. His current work has focused on the development of dynamic models of isolated power systems, the integration of renewable energy sources, and their effects on frequency control. He has also studied energy storage systems, such as pumped-storage hydropower and flywheel energy storage, and proposed control strategies for technologies, including variable-speed wind turbines. He has authored or co-authored more than 20 journal articles indexed in JCR. His research has included case studies in the Canary Islands (El Hierro, Gran Canaria, La Palma, and Tenerife).

Dr. Sarasua has been a member of the EERA Joint Program on Energy Storage, since 2016, and the EERA Joint Program on Hydropower, since 2019.